




Uncharacterized Bacterial Structures Revealed by Electron Cryotomography

Megan J. Dobro,^a Catherine M. Oikonomou,^b Aidan Piper,^a John Cohen,^a Kylie Guo,^b Taylor Jensen,^b Jahan Tadayon,^b Joseph Donermeyer,^b Yeram Park,^b Benjamin A. Solis,^c Andreas Kjær,^d Andrew I. Jewett,^b Alasdair W. McDowall,^b Songye Chen,^b Yi-Wei Chang,^b Jian Shi,^e Poorna Subramanian,^b Cristina V. Iancu,^f Zhuo Li,^g Ariane Briegel,^h Elitza I. Tocheva,ⁱ Martin Pilhofer,^j  Grant J. Jensen^{b,k}

Hampshire College, Amherst, Massachusetts, USA^a; California Institute of Technology, Pasadena, California, USA^b; University at Albany, SUNY, Albany, New York, USA^c; University of Southern Denmark, Odense, Denmark^d; National University of Singapore, Singapore, Republic of Singapore^e; Rosalind Franklin University of Medicine and Science, Chicago, Illinois, USA^f; City of Hope, Duarte, California, USA^g; Leiden University, Sylvius Laboratories, Leiden, Netherlands^h; University of Montreal, Montreal, Quebec, Canadaⁱ; ETH Zurich, Zurich, Switzerland^j; Howard Hughes Medical Institute, Pasadena, California, USA^k

ABSTRACT Electron cryotomography (ECT) can reveal the native structure and arrangement of macromolecular complexes inside intact cells. This technique has greatly advanced our understanding of the ultrastructure of bacterial cells. We now view bacteria as structurally complex assemblies of macromolecular machines rather than as undifferentiated bags of enzymes. To date, our group has applied ECT to nearly 90 different bacterial species, collecting more than 15,000 cryotomograms. In addition to known structures, we have observed, to our knowledge, several uncharacterized features in these tomograms. Some are completely novel structures; others expand the features or species range of known structure types. Here, we present a survey of these uncharacterized bacterial structures in the hopes of accelerating their identification and study, and furthering our understanding of the structural complexity of bacterial cells.

IMPORTANCE Bacteria are more structurally complex than is commonly appreciated. Here we present a survey of previously uncharacterized structures that we observed in bacterial cells by electron cryotomography, structures that will initiate new lines of research investigating their identities and roles.

KEYWORDS bacteria, electron cryotomography, bacterial ultrastructure, uncharacterized structures, electron microscopy

The history of cell biology has been punctuated by advances in imaging technology. In particular, the development of electron microscopy (EM) in the 1930s produced a wealth of new information about the ultrastructure of cells (1). For the first time, the structure of cell envelopes, internal organelles, cytoskeletal filaments, and even large macromolecular complexes like ribosomes became visible. A further advance came in the 1980s and 1990s with the development of electron cryotomography (ECT) (2), which allows small cells to be imaged intact in 3D in a near-native, “frozen-hydrated” state to “macromolecular” (~5 nm) resolution, without the limitations and artifacts of more traditional specimen-preparation methods (3).

ECT has helped reveal the previously unappreciated complexity of “simple” bacterial cells. Our group has been using ECT to study bacteria for more than a decade, generating more than 15,000 tomograms of 88 different species. These tomograms have revealed new insights into, among other things, the bacterial cytoskeleton (4–7), cell wall architecture (8, 9), morphogenesis (10), metabolism (11), motility (12–15),

Received 10 March 2017 Accepted 27 May 2017

Accepted manuscript posted online 12 June 2017

Citation Dobro MJ, Oikonomou CM, Piper A, Cohen J, Guo K, Jensen T, Tadayon J, Donermeyer J, Park Y, Solis BA, Kjær A, Jewett AI, McDowall AW, Chen S, Chang Y-W, Shi J, Subramanian P, Iancu CV, Li Z, Briegel A, Tocheva EI, Pilhofer M, Jensen GJ. 2017. Uncharacterized bacterial structures revealed by electron cryotomography. *J Bacteriol* 199:e00100-17. <https://doi.org/10.1128/JB.00100-17>.

Editor Thomas J. Silhavy, Princeton University

Copyright © 2017 American Society for Microbiology. All Rights Reserved.

Address correspondence to Grant J. Jensen, jensen@caltech.edu.

chemotaxis (16), sporulation (17), cell-cell interactions (18), and phage infection (19) (for a summary with more references from our and others' work, see reference 20).

A major hurdle in such studies is identifying the novel structures observed in tomograms. In some cases, we have identified structures by perturbing the abundance (either by knockout or overexpression) of candidate proteins (21). In others, we have used correlated light and electron microscopy (CLEM) to locate tagged proteins of interest (22, 23). In one striking example, we observed 12- and 15-nm-wide tubes in our tomograms of *Vibrio cholerae* cells. Ultimately, in collaboration with John Mekalanos' group, we identified them as type VI secretion systems (T6SS), which immediately led to the insight that the bacterial T6SS functions as a phage-tail-like, contractile molecular dagger (18).

Many other novel structures we have observed, though, remain unidentified. In some cases, we have published papers describing the novel structures seen in a particular species (e.g., references 24 and 25), but many have never been published. We therefore conducted a visual survey of the tomograms collected by our group, curated in the Caltech Tomography Database (26), as of 2015 and present here a catalog of previously undescribed bacterial structures. Some structures are, to our knowledge, completely novel; others belong to known types but present additional features or an expanded species range. We hope that sharing these images will help spur their identification and study, contributing to our expanding understanding of bacterial cell biology. In addition, we look forward to a future in which custom microbes are designed for diverse medical and industrial purposes; an expanded "parts list" of structures to be repurposed will aid in this effort.

RESULTS AND DISCUSSION

We performed a visual inspection of approximately 15,000 tomograms of intact frozen-hydrated cells belonging to 88 species and identified what we believed to be novel structures. A summary of the results of this survey is shown in Table S1 in the supplemental material, with features observed, species range, and frequency listed for each structure type. For full tomographic (3D) views of each feature, see reference 27; to view the figures in virtual reality, see reference 75.

Extracellular structures: external appendages. *Prostheco bacter debontii* is a bacterial species from the poorly studied phylum *Verrucomicrobia*. Each vibroid *P. debontii* cell possesses an appendage (prostheca), similar to the stalk of *Caulobacter crescentus* (28). In several tomograms of *P. debontii*, we observed novel extracellular appendages along the prosthecae, apparently attached to the cell membrane. Individual cells displayed up to 30 such appendages, which exhibited consistent sizes (~20 nm wide and ~50 nm long) and shapes (Fig. 1A). Subtomogram averaging of 105 particles revealed a distinctive structure. Extending outward from the cell membrane, five legs were attached to a disc, which in turn connected to a smaller disc and a long neck region (Fig. 1B and C). Individual particles showed that the structure culminated in two antenna-like filaments, which were likely lost in the average due to conformational variability. The appendages were observed in multiple cultures of the strain. While it remains unclear whether they originated intracellularly or extracellularly, no free-floating appendages were ever observed in the extracellular space. They may represent novel bacterial attachment organelles or appendages for nutrient acquisition, which has been proposed for a similar structure, the *Caulobacter* stalk. Under phosphate-limited conditions, *Caulobacter* grew elongated stalks (29). This increase in cell surface area with respect to cell volume was hypothesized to allow increased phosphate uptake (30). However, the presence of diffusion barriers challenges this view (31). The appendages could also be a novel secretion system (though we might expect a cell envelope spanning complex) or a novel bacteriophage (though there is a notable lack of a capsid-like density).

We observed a different novel extracellular appendage in tomograms of cell poles of *Azospirillum brasilense*, a plant growth-promoting bacterium of the *Alphaproteobacteria* class with a curved-rod morphology. Thin hooks were seen extending from the cell

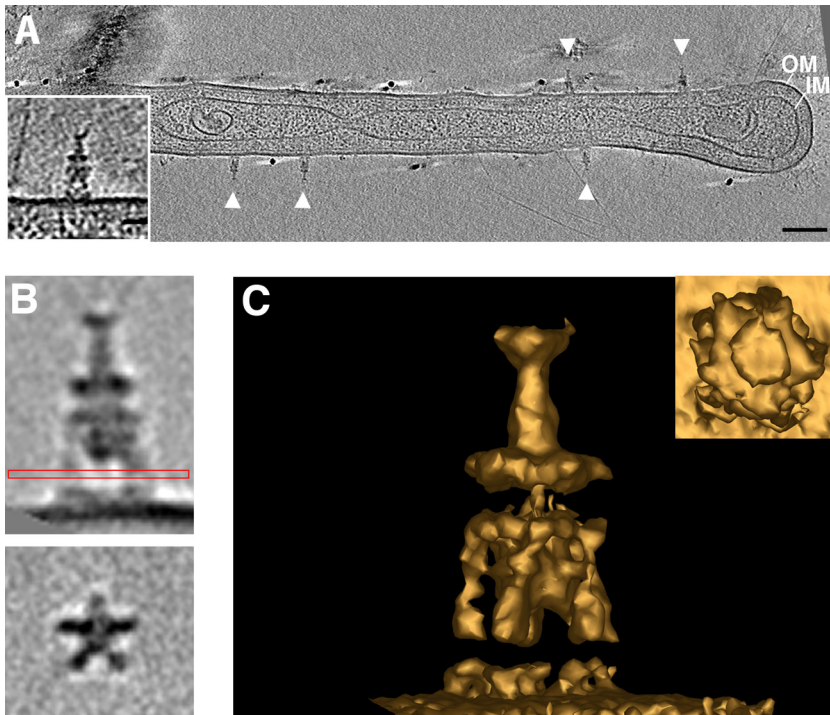


FIG 1 Novel *Prosthecobacter debontii* appendages. Multiple external appendages (arrowheads) were observed by ECT on *P. debontii* prosthecae. (A) A central tomographic slice is shown, with a single appendage enlarged in the inset. Subtomogram averaging revealed the structure in more detail. (B) Side (top) and top (bottom) views show the characteristic disc-like densities and the five legs attaching to the cell surface. The red box shows which view was used to rotate the image 90° for the bottom image. (C) 3D isosurface of the average, seen from the side and top (inset). Bars, 50 nm (A) and 20 nm (inset).

surface (Fig. 2). Individual cells exhibited dozens of hooks, each ~3 nm wide and ~75 nm long, associated with the outer membrane. The cells are large, and most tomograms included only the cell pole region, so while hooks were observed only at the pole region, they may also occur elsewhere on the cell. Hooks were seen in >90% of wild-type cells as well as in a strain in which the operon encoding the Che1 chemotaxis system was deleted. They were seen in ~50% of cells in which the Che4 chemotaxis system operon was deleted, and none were seen in cells lacking both the Che1 and

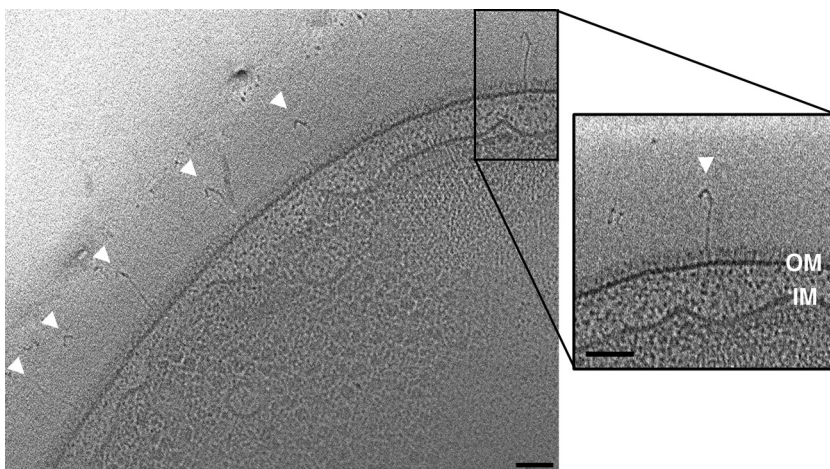


FIG 2 Novel *Azospirillum brasilense* hooks. Many hook-like structures were observed on the surface of *A. brasilense* cells. A central tomographic slice is shown, with arrowheads indicating hooks. A single hook is shown enlarged at right. Bars, 50 nm.

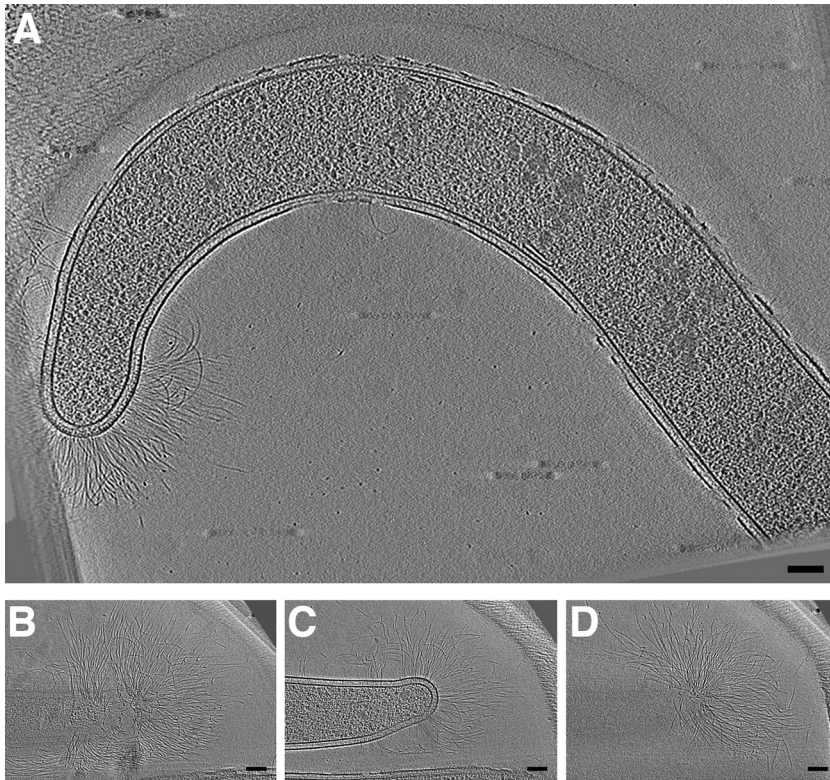


FIG 3 Strain JT5 fimbriae. Examples are shown from two cells of strain JT5 (related to the *Dysgonomonas* genus) exhibiting abundant fimbriae at the cell pole. (A) Central slice revealing overall cell morphology; (B to D) slices at progressive z-heights through a cryotomogram of a cell of strain JT5 (related to the *Dysgonomonas* genus). Abundant fimbriae can be seen at the cell pole. Bars, 100 nm.

Che4 operons. *A. brasilense* is a well-studied plant growth-promoting bacterium. Cells attach to plant roots through a two-step process (32), a rapid reversible adsorption, thought to be mediated by the polar flagellum, and a slow irreversible anchoring, thought to be mediated by an as-yet unidentified surface polysaccharide (33). A recent study reported that mutants in components of the Che4 chemotaxis system are defective in this root colonization (34). *A. brasilense* cells also attach to conspecifics in the presence of elevated oxygen levels (35). Interestingly, it has been shown that mutants in components of the Che1 chemotaxis system form such attachments more rapidly than wild-type cells (36). The hooks we observed are vaguely reminiscent of the grappling hook-like structures that an archaeal species uses to anchor itself in biofilms (37), though those hooks were longer fibers with barbs. Those archaeal cells demonstrated very strong adhesion to a variety of surfaces as well as to each other. It is tempting, therefore, to speculate that the hooks shown here play a similar role in adhesion, to either other *A. brasilense* cells or plant roots.

In cells of strain JT5 (a rod-shaped bacterium isolated from termite gut and related to the *Dysgonomonas* genus), we observed abundant fimbriae concentrated at the cell poles (Fig. 3). Fimbriae were also observed at the cell body but were much more concentrated at the cell poles. They were present in cells grown on cellulose or xylan, as well as under a starvation-inducing condition. Their width (~4 nm), apparent flexibility, density on the cell envelope, and inhomogeneous distribution around the cell is consistent with curli, functional amyloids secreted by the type VIII secretion system that are involved in adhesion (38, 39). Curli systems are relatively divergent at the sequence level but are remarkably widespread phylogenetically, and the genes were reported to be present in *Bacteroidetes* (the phylum containing *Dysgonomonas*) (40). The appendages we observed in strain JT5 may therefore play a role in adhesion in the environment of the termite gut.

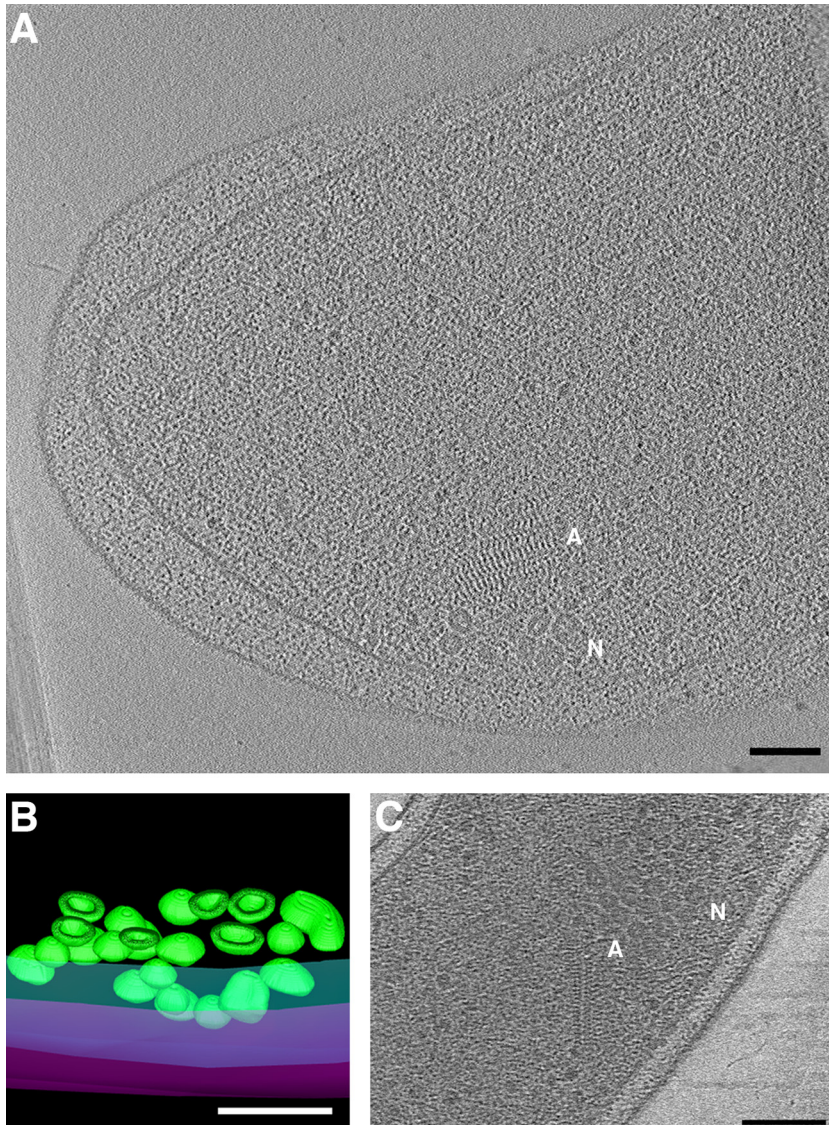


FIG 4 Novel *Vibrio cholerae* nanospheres. Clusters of nanospheres were observed in two cryotomograms of *V. cholerae* cells (central slices shown in panels A and C). “N” indicates nanospheres; “A” indicates associated filament array. (B) Segmentation of the cluster seen in panel A, with outer and inner membranes in magenta and cyan, respectively, and nanospheres in green. A clipping plane cuts through the 3D segmentation revealing the thick walls and hollow centers of the nanospheres. Bars, 100 nm.

Intracellular structures. (i) Nanospheres. In two *Vibrio cholerae* cells (one from a C6706 *lacZ* mutant [41] and one from a $\Delta ctxA \Delta tcpB$ strain [15]) we observed clusters of nanospheres, hollow granules with thick walls (Fig. 4). The diameter of the nanospheres ranged from ~ 18 to 37 nm, and the walls were ~ 4 to 10 nm thick. They were pleomorphic; most were roughly spherical, but some were oblong or comma shaped. Each cluster contained about two dozen nanospheres. The clusters were observed at the cell periphery, near the inner membrane (although the clusters were large enough to extend to the center of the cell), and were always observed near a filament array structure (discussed below).

(ii) Filaments, bundles, arrays, chains and meshes. One of the strengths of ECT imaging is its power to resolve cytoskeletal elements in small bacterial cells. In addition to those we have already identified, we observed many novel filamentous structures in tomograms, including filament arrays, bundles, chains, and meshes (Fig. 5). In *Hyphomonas neptunium*, we observed long helical filament bundles in the prosthecae that

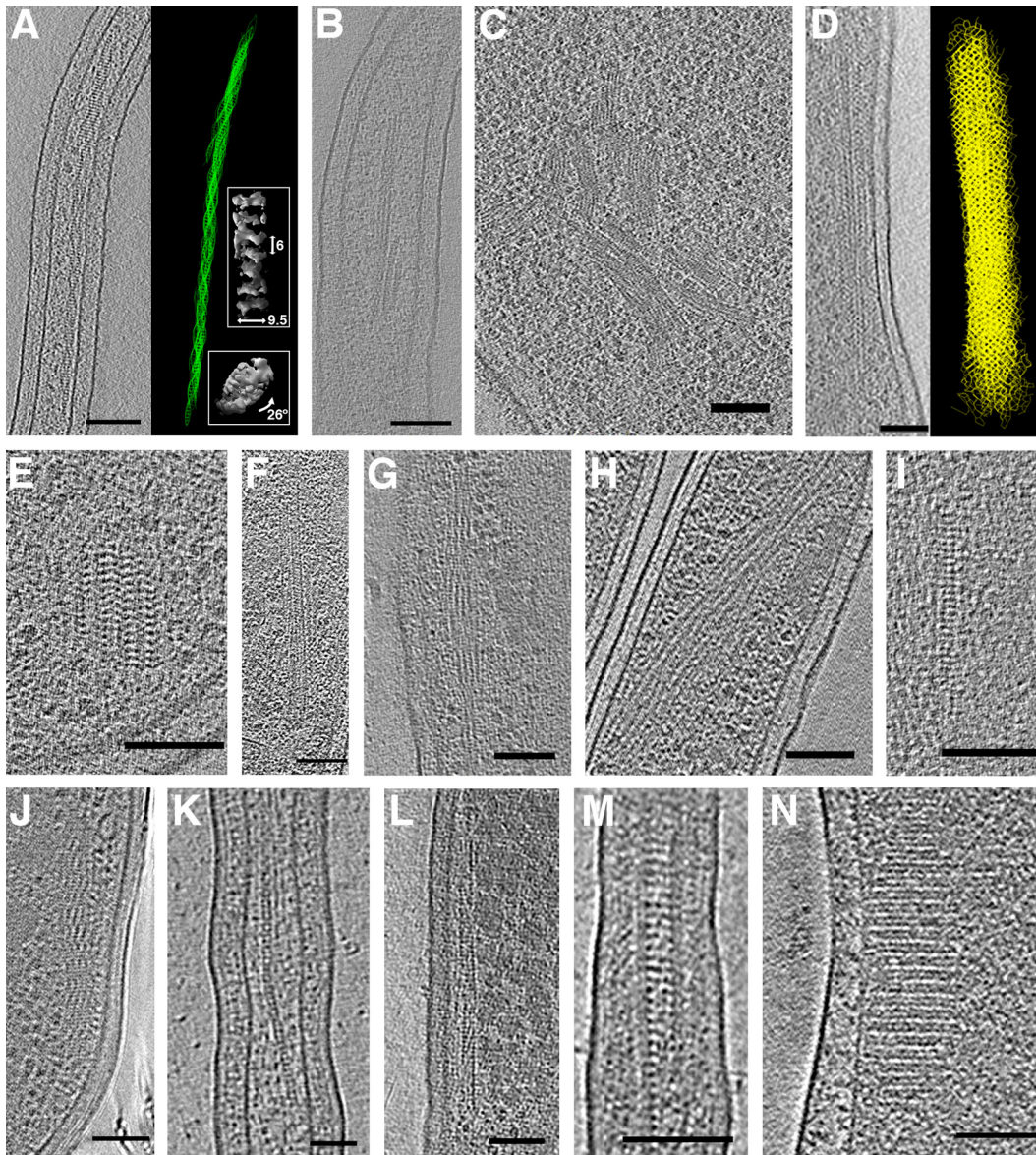


FIG 5 Filament bundles, arrays, and chains. *Hyphomonas neptunium* division stalks contained helical bundles (A) that straightened when cells were treated with ethidium bromide (B). The right side of panel A shows a 3D segmentation of the helical bundle, with side and top views of subtomogram averaged insets. Labeled dimensions are in nanometers. (C) Large filament bundles in *Helicobacter pylori*. (D) A long mesh-like filament array in *Vibrio cholerae*, with segmentation at right. (E) A more typical *V. cholerae* filament array. (F to J) Filament arrays in *Thiomonas intermedia* (F), *Hyphomonas neptunium* (G), *Hylemonella gracilis* (H), *Halothiobacillus neapolitanus* c2 (I), and *Mycobacterium smegmatis* (J). (K) A chain in *Prosthecobacter vanneervanii*. (L to M) Filament arrays in *Prosthecobacter debontii*. (N) A filament array in a starved *Campylobacter jejuni* cell. Bars, 100 nm (A, B, D to J, L to N) and 50 nm (C and K).

connect dividing cells (Fig. 5A). The helix width was 9.5 ± 1.5 nm, the spacing between cross-densities 6.0 ± 0.3 nm, and the helical pitch was $\sim 26^\circ$. *H. neptunium* divides by asymmetric budding (42), and the genome of the parent cell is passed to the daughter cell through the narrow prostheca connecting the two cells (43). We observed that the helical structure was straightened in cells treated with ethidium bromide (an intercalator known to unwind DNA [44]) (Fig. 5B). We therefore propose that the helix is composed of supercoiled DNA, with each visible filament a DNA duplex connected to adjacent duplexes by cross-densities formed by an unidentified protein.

In *Helicobacter pylori* cells, we observed extensive filament bundles. In one cell in an early stage of lysis, such bundles were observed throughout most of the cell (Fig. 5C). In *V. cholerae* we observed filament arrays resembling a honeycombed mesh (Fig. 5D).

These arrays varied in length but were usually fairly short (~ 100 nm in length and width), like the example shown in Fig. 5E. This is the structure we observed near the nanosphere clusters. Filament arrays exhibited different morphologies in other species. *Thiomonas intermedia* cells contained untwisted arrays that were ~ 48 nm thick and ~ 30 nm wide (Fig. 5F). In addition to the prosthecal helix described above, *H. neptunium* cells also contained a bundle of twisting filaments laddered by cross-densities (Fig. 5G). These bundles were ~ 40 nm thick and ~ 75 nm wide. In a *Hylemonella gracilis* cell we observed a helical bundle of filaments that varied in width and could be related to the nucleoid (Fig. 5H). In *Halothiobacillus neapolitanus* c2 cells grown in limited CO₂ for several hours, we observed linear filament arrays with prominent cross-densities spaced 7 ± 0.8 nm apart (Fig. 5I). *Mycobacterium smegmatis* displayed straight arrays ~ 80 nm thick and wide, comprising segments of pitched filaments (Fig. 5J). Filament arrays were also seen in multiple species of *Prostheco bacter*; *P. vanneervanii* contained linear chains (Fig. 5K), and one *P. debontii* cell contained a straight array similar to those observed in *T. intermedia* (Fig. 5L), as well as mesh-like arrays spanning the width of the prostheca (Fig. 5M).

In starving *Campylobacter jejuni* cells, we observed regular filament arrays (Fig. 5N). When subjected to environmental or cellular stress, some bacteria, including *Escherichia coli*, have been shown to reorganize their DNA into protective crystalline arrays (45). Since then, additional nucleoid associated proteins have been identified that organize DNA into higher order structures in stationary-phase or stress conditions (46, 47). The structures we observed in *C. jejuni* resemble those seen in *E. coli* cells overexpressing the protective DNA binding protein Dps (45) and may, therefore, represent such a nucleoprotein array.

Several other proteins have been shown to copolymerize with DNA into filaments for various functions, including RecA (homologous recombination) (48) and MuB from bacteriophage Mu (DNA transposition) (49). The width of such filaments *in vitro* (~ 10 nm) is similar to widths we observed in cells; it is possible that some of the structures in Fig. 5 represent these DNA-related processes. Other bacterial proteins form filaments to regulate their function, and it has been suggested that this property may have been coopted in the evolution of the cytoskeleton (50). We previously observed such filaments of CTP synthase in tomograms of *C. crescentus* cells (21). Another protein, alcohol dehydrogenase, forms plaited filaments ~ 10 nm wide, called spiroosomes, in many bacteria capable of anaerobic metabolism (51, 52). It is possible that some of the filament arrays and chains that we observed in tomograms were filaments formed by these or other, yet uncharacterized, proteins.

In addition to filament arrays and bundles, we observed individual or paired filaments in nearly every species imaged. Examples are shown in Fig. 6. (Note that due to their ubiquity, statistics are not included in Table S1 in the supplemental material.) Filaments were seen with various orientations in the cytoplasm (Fig. 6A to C), as well as running alongside the membrane (Fig. 6D and E). Consistent with our previous work (53), we did not observe any filaments immediately adjacent to the membrane as predicted by some studies of MreB (e.g., references 54 and 55). (Note that we did observe filaments corresponding to the known types of MamK [4, 56], FtsZ [5, 57], and bactofilins [58] but we do not show them here since they have already been characterized.) Paired filaments have been shown to function in plasmid segregation, so it is possible that some paired filaments that we observed were such ParM or TubZ structures (59, 60).

(iii) Tubes. In addition to the known types of tubes we reported earlier, such as bacterial microtubules (6) and type VI secretion systems (18), we observed several novel tubular structures in bacterial cells (Fig. 7). In *Thiomicrospira crunogena* we found large tubes (18.6 ± 1.8 nm in diameter) containing eight outer protofilaments surrounding a central protofilament (Fig. 7A). *H. neapolitanus* c2 cells also contained large tubes (16.7 ± 0.7 nm in diameter) with a central filament (Fig. 7B). In several other species, we observed hollow tubes of varying dimensions: 8.9 ± 0.3 nm in diameter in *Bdellovibrio*

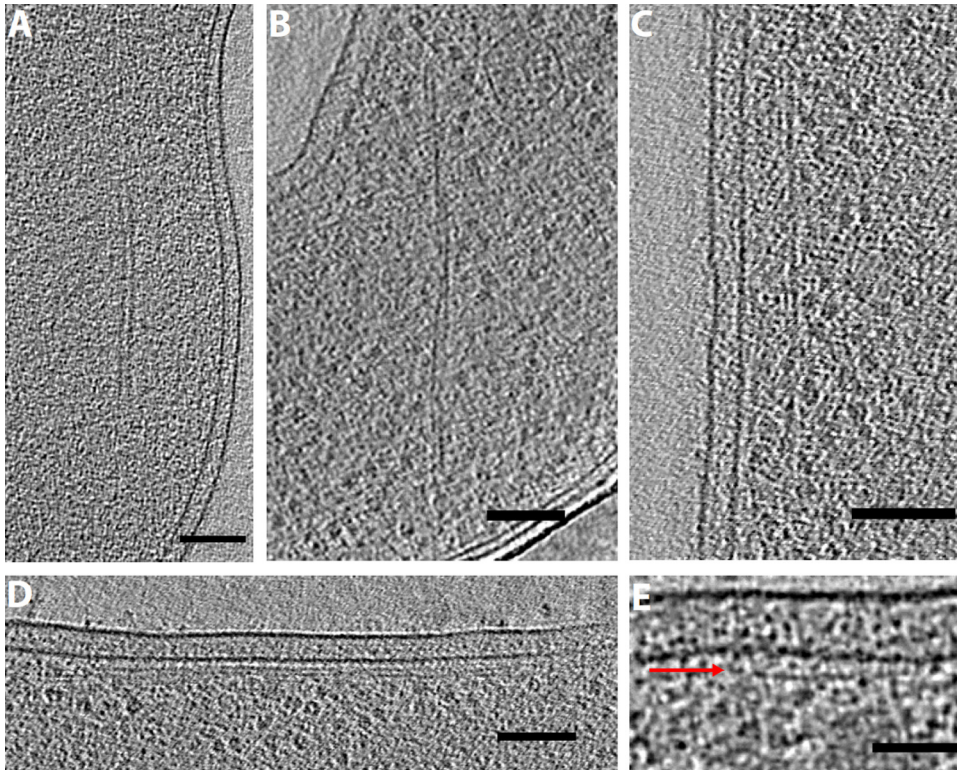


FIG 6 Single and paired filaments. Tomographic slices showing paired filaments in *Campylobacter jejuni* (A) and *Thiomicrospira crunogena* (B) and membrane-aligned filaments in *Shewanella putrefaciens* (C), *Prosthecobacter debontii* (D), and *Prosthecobacter fluviatilis* (E) (the arrow shows a filament just under the inner membrane). Bars, 100 nm (A to D) and 50 nm (E).

bacteriovorus (Fig. 7C), 14.3 ± 1.7 nm in *T. intermedia* (Fig. 7D), and 8.3 ± 0.5 nm in *H. neptunium* (Fig. 7E). *H. neptunium* cells also contained many rings of similar diameter. In fact, we observed rings in many species, which could be assembly or disassembly intermediates of tubes.

In addition to isolated rings, in one case we observed an organized array of rings. One slightly lysed (a condition that flattens the cell and increases image quality) *H. pylori* cell contained a striking array of about two dozen evenly spaced rings near the cytoplasmic membrane (Fig. 7F). Each ring was ~ 6 nm in diameter and ~ 20 nm (center-to-center distance) from its neighbors in the square lattice.

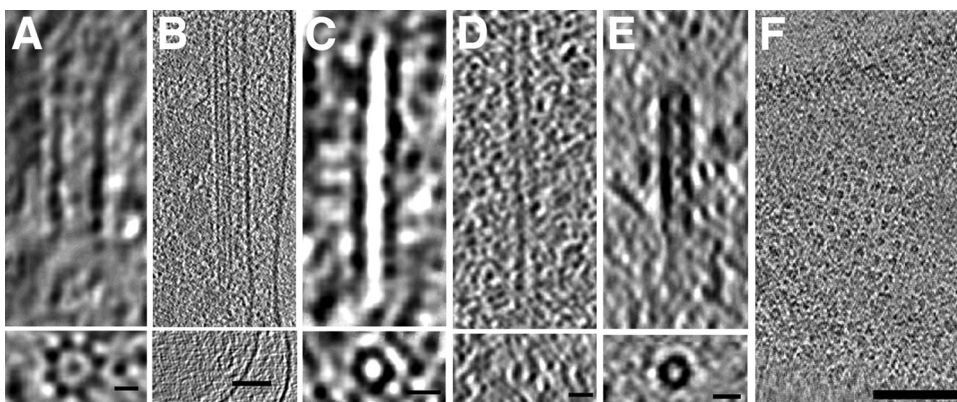


FIG 7 Tubes and rings. Tubes observed in *Thiomicrospira crunogena* (A), *Halothiobacillus neapolitanus* c2 (B), *Bdellovibrio bacteriovorus* (C), *Thiomonas intermedia* (D), and *Hyphomonas neptunium* (E). In each panel, tomographic slices show a side view (above) and a top view (bottom). (F) An array of rings observed in *Helicobacter pylori*. Bars, 10 nm (A, C, and E), 20 nm (B and D), and 100 nm (F).

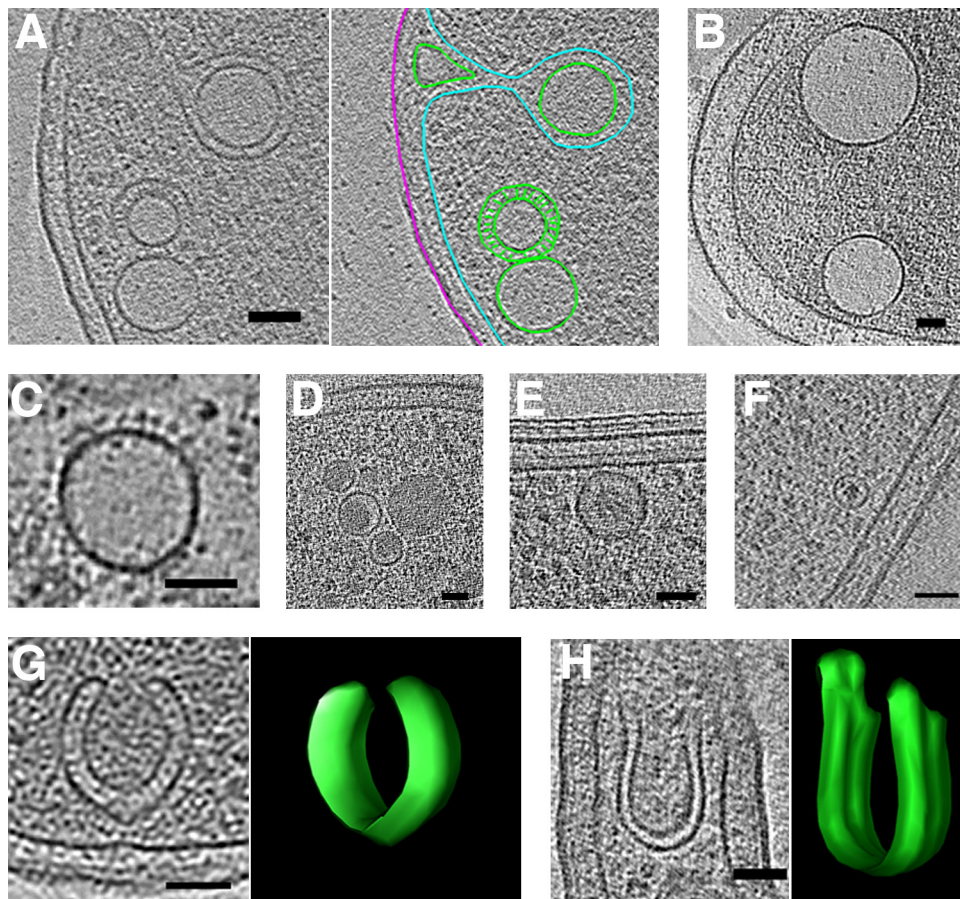


FIG 8 Round and horseshoe-shaped vesicles. Tomographic slices showing examples of round vesicles in *Escherichia coli* (A) (segmentation shown at right), *Helicobacter pylori* (B), *Helicobacter hepaticus* (C), *Myxococcus xanthus* (D), *Caulobacter crescentus* (E), and *Myxococcus xanthus* overexpressing PilP-sfGFP (F). Examples of horseshoe-shaped vesicles in *Ralstonia eutropha* (G) and *Prosthecobacter fluviatilis* (H), with 3D segmentations shown at right. In the segmentation in panel A, outer and inner membranes are in magenta and cyan, respectively, and vesicles are in green. Bars, 50 nm.

(iv) Vesicles. In contrast to eukaryotic cells, relatively little is known about membrane remodeling in bacteria. Compartmentalized cells in the *Planctomycetes-Verrucomicrobia-Chlamydiae* (PVC) superphylum have been shown to contain homologs of eukaryotic membrane trafficking proteins (61) and exhibit endocytosis-like protein uptake (62). An additional potential membrane-remodeling system based on FtsZ homologues is more widespread across bacteria, but its function remains unknown (63).

Despite this limited evidence for membrane remodeling in bacteria, we observed intracellular vesicles in nearly every species imaged. They exhibited various sizes, shapes, membrane layers, and contents and were frequently found near the cytoplasmic membrane. Figure 8 shows examples of round and horseshoe-shaped vesicles. Round vesicles were found in nearly every species imaged; therefore, no statistics for them are compiled in Table S1 in the supplemental material. Most round vesicles were empty (density similar to background [e.g., Fig. 8A to C]). One of these vesicles, observed in a lysed cell (improving clarity by reducing cytoplasmic crowding), exhibited regularly spaced protein densities around its exterior (Fig. 8C). Others were at least partially filled with denser material (e.g., Fig. 8D to F). In two *Myxococcus xanthus* cells overexpressing a fluorescent fusion of a periplasmic protein (PilP-sfGFP), we observed round vesicles containing a dense amorphous core (Fig. 8F). These could be a novel form of membrane-bound inclusion bodies, perhaps packaged from the periplasm. In eight species, we observed horseshoe-shaped vesicles (Fig. 8G and H).

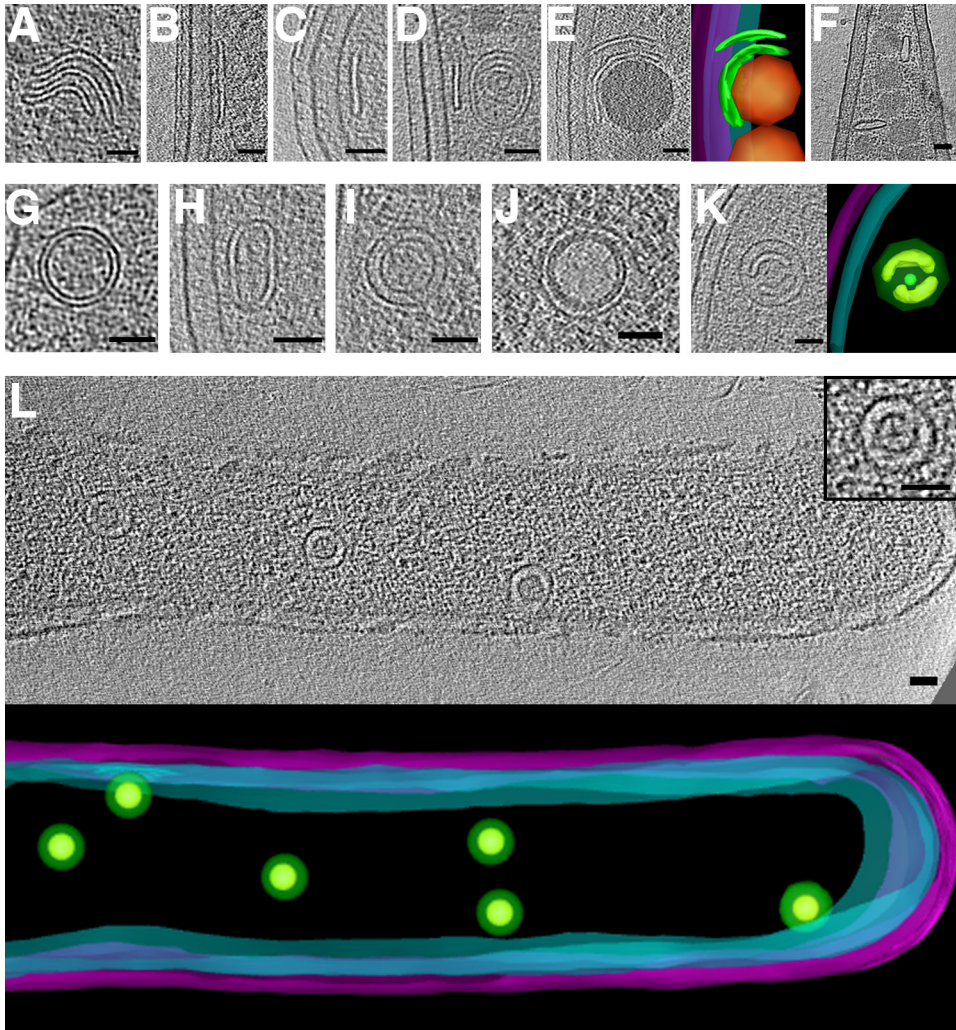


FIG 9 Flattened and nested vesicles. Examples of flattened vesicles in *Thiomonas intermedia* (A), *Caulobacter crescentus* (B to E), and *Prosthecobacter debontii* (F). Note storage granules in panels E and F, shown in orange in the segmentation panel E (G to L). Examples of nested vesicles in *Serpens flexibilis* (G), *Caulobacter crescentus* (H), *Borrelia burgdorferi* (I), *Vibrio cholerae* (J), *Caulobacter crescentus* with segmentation (K), and strain JT5 (L). (L, inset) Shows an enlargement of central vesicle, and a 3D segmentation of the visible portion of the cell is shown below. In segmentations, outer and inner membranes are shown in magenta and cyan, respectively, and vesicles are in green. Bars, 50 nm.

Flattened vesicles (Fig. 9A to F) were less common than round vesicles, and were usually observed near membranes or wrapping around storage granules (Fig. 9E), suggesting a possible functional relationship. Flattened vesicles were usually empty. One *T. intermedia* cell contained a stack of flattened vesicles (Fig. 9A). Flattened vesicles were particularly prevalent in *C. crescentus* cells (Fig. 9B to E). *P. debontii* cells contained flattened vesicles that neither ran along the membrane nor wrapped around granules (Fig. 9F). Since the lowest energy shape of a liposome is a sphere, it is likely that the vesicles were flattened by cytoplasmic pressure or some other constraint such as an associated protein.

Many cells contained nested vesicles, with diverse sizes and shapes, as well as subcellular locations (Fig. 9G to L). In some nested vesicles, densities were observed bridging the inner and outer membranes (Fig. 8A and 9G and H). Cells of strain JT5 exhibited multiple nested vesicles of uniform shape and size (Fig. 9L).

We also observed periplasmic vesicles in many species (Fig. 10). They were typically empty and exhibited great variability in size, shape, and abundance. In some cases, they were even seen to form branching networks (Fig. 10A). As with cytoplasmic vesicles,

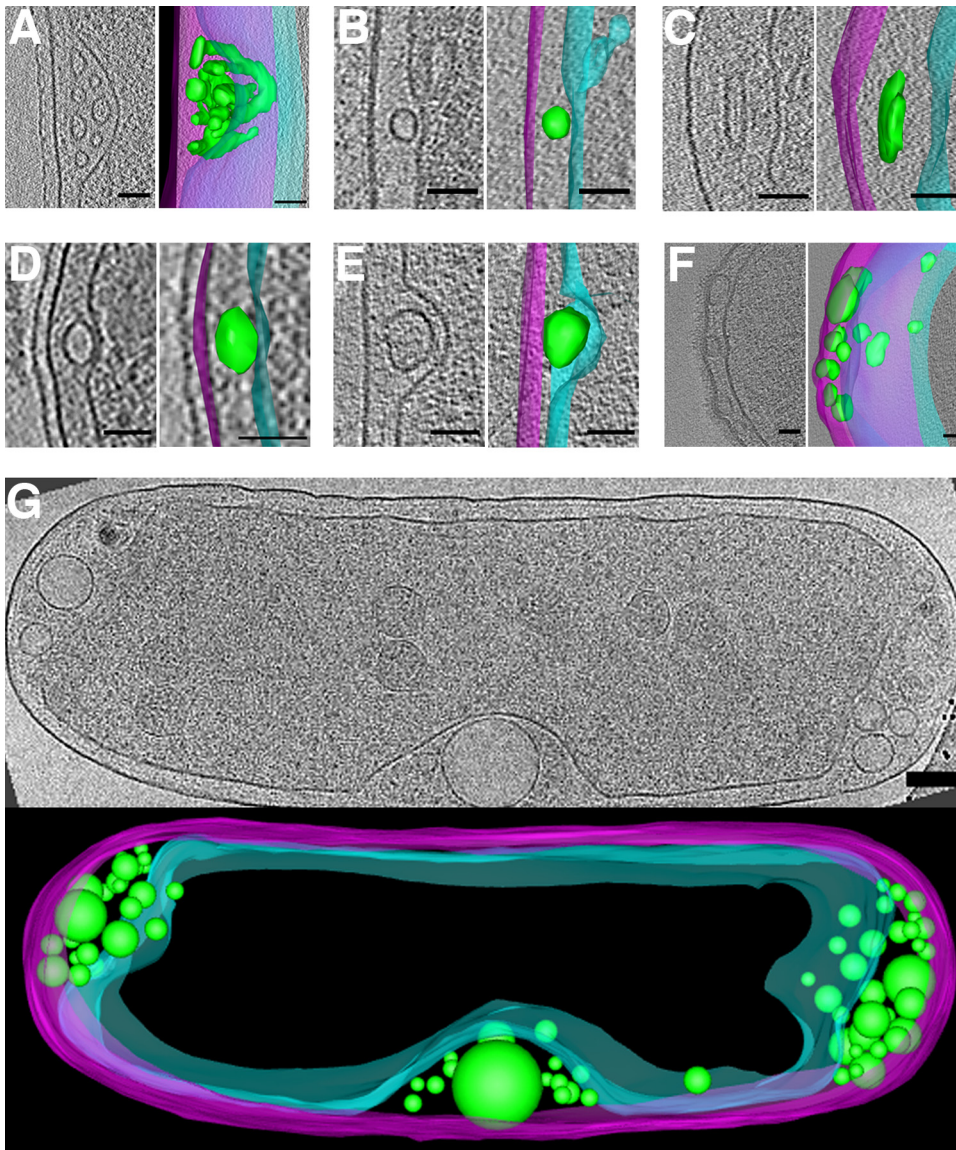


FIG 10 Periplasmic vesicles. Examples of periplasmic vesicles in *Caulobacter crescentus* (A), *Helicobacter pylori* (B), *Brucella abortus* (C), *Thiomonas intermedia* (D), *Hyphomonas neptunium* (E), *Myxococcus xanthus* (F), and *Halothibacillus neapolitanus* c2 (G). In each panel, a central tomographic slice is shown, as well as a segmentation with outer and inner membranes in magenta and cyan, respectively, and vesicles are in green. Bars, 50 nm (A to F) and 100 nm (G).

they were most abundant in cells showing signs of stress (rupture of inner or outer membrane, separation of inner and outer membrane, lysis, or membrane blebbing).

Conclusions. Here we present the results of a survey of, to our knowledge, uncharacterized bacterial structures that we have observed in our work over the past 10 or more years. We hope that further study will identify them and their functions. Already, they signal the wealth of complexity still to be discovered in bacterial cells.

MATERIALS AND METHODS

Strains and growth. Unless otherwise noted, bacterial strains were wild type and grown in species-standard medium and conditions to mid-log or early stationary phase. *Azospirillum brasilense* cultures were switched to nitrogen-free medium for ~16 h prior to imaging to induce nitrogen fixation and digestion of storage granules that decrease image quality. Predatory *Bdellovibrio bacteriovorus* cells were cocultured with *Vibrio cholerae* strain MKW1383. *Helicobacter pylori* cells were cultured with human gastric carcinoma cells. *Vibrio cholerae* and *Borrelia burgdorferi* were grown according to conditions in references 64 and 65). *E. coli* were grown according to conditions in references 16 and 66). *Caulobacter*

crescentus were grown according to conditions in reference 67. Prosthecobacters were all grown according to conditions in reference 6. *Hyphomonas neptunium* was grown according to conditions in reference 68.

In all cases, samples of cells in growth medium were mixed with BSA-treated 10 nm colloidal gold fiducials (Sigma), applied to glow-discharged EM grids (Quantifoil), and plunge-frozen in a liquid ethane-propane mixture (69). Grids were maintained at liquid nitrogen temperature throughout storage, transfer, and imaging.

Electron cryotomography. The references to growing conditions above also provide specific data collection settings. Generally, plunge-frozen samples were imaged using either a Polara or Titan Krios 300 kV FEG transmission electron microscope (FEI Company) equipped with an energy filter (Gatan). Images were recorded using either a lens-coupled 4,000 by 4,000 UltraCam CCD (Gatan) or a K2 Summit direct electron detector (Gatan). Tilt-series were recorded from -60° to $+60^\circ$ in 1 to 2° increments, with defoci of ~ 6 to $12 \mu\text{m}$ and a cumulative dose of ~ 100 to $200 \text{ e}^-/\text{\AA}^2$. Tilt-series were acquired automatically using either Legikon (70) or UCSF Tomography (71) software. Tomographic reconstructions were calculated using either the IMOD software package (72) or Raptor (73). 3D segmentations and movies were produced with IMOD (72). Subtomogram averages were calculated using PEET software (74).

SUPPLEMENTAL MATERIAL

Supplemental material for this article may be found at <https://doi.org/10.1128/JB.00100-17>.

SUPPLEMENTAL FILE 1, PDF file, 0.1 MB.

ACKNOWLEDGMENTS

We thank our collaborators who provided strains for imaging: Andrew Camilli (*Streptococcus pneumoniae*), Eric Matson (strain JT5), Gladys Alexandre (*Azospirillum brasilense* mutants), Lotte Sogaard-Andersen, Simon Ringgaard, and Matthew K. Waldor (*Vibrio cholerae* wild type and mutants), Michael Marletta (*Shewanella putrefaciens*), and Gordon Cannon and Sabine Heinhorst (*Halothiobacillus neapolitanus* and *Thiomonas intermedia*). We also thank members of the Jensen lab for their helpful discussions.

We declare no competing interests.

M.J.D. and G.J.J. conceived the idea for the study; M.J.D., C.M.O., A.P., J.C., K.G., T.J., J.T., J.D., Y.P., A.K., A.I.J., M.P., S.C., E.I.T., Y.-W.C., A.B., J.S., Z.L., P.S., C.V.I., B.A.S., and A.W.M. performed formal analysis and investigation; M.J.D. and C.M.O. wrote and prepared the original article draft; M.J.D., C.M.O., and G.J.J. wrote, reviewed, and edited the final article draft; M.J.D. and G.J.J. acquired funding; G.J.J. provided resources; and M.J.D. and G.J.J. supervised the study.

This work was supported by the Hampshire College Dr. Lucy fund and the Collaborative Modeling Center, NIH grant R01 AI27401 (to G.J.J.), the Beckman Institute at Caltech, the Gordon and Betty Moore Foundation, the Human Frontier Science Program, the Howard Hughes Medical Institute, and the John Templeton Foundation as part of the Boundaries of Life project.

The opinions expressed in this publication are those of the authors and do not necessarily reflect the views of the John Templeton Foundation.

REFERENCES

- Ruska E. 1987. Nobel lecture. The development of the electron microscope and of electron microscopy. *Biosci Rep* 7:607–629.
- Koster AJ, Grimm R, Typke D, Hegerl R, Stoschek A, Walz J, Baumeister W. 1997. Perspectives of molecular and cellular electron tomography. *J Struct Biol* 120:276–308. <https://doi.org/10.1006/jsbi.1997.3933>.
- Pilhofer M, Ladinsky MS, McDowell AW, Jensen GJ. 2010. Bacterial TEM: new insights from cryo-microscopy. *Methods Cell Biol* 96:21–45. [https://doi.org/10.1016/S0091-679X\(10\)96002-0](https://doi.org/10.1016/S0091-679X(10)96002-0).
- Komeili A, Li Z, Newman DK, Jensen GJ. 2006. Magnetosomes are cell membrane invaginations organized by the actin-like protein MamK. *Science* 311:242–245. <https://doi.org/10.1126/science.1123231>.
- Li Z, Trimble MJ, Brun YV, Jensen GJ. 2007. The structure of FtsZ filaments in vivo suggests a force-generating role in cell division. *EMBO J* 26:4694–4708. <https://doi.org/10.1038/sj.emboj.7601895>.
- Pilhofer M, Ladinsky MS, McDowell AW, Petroni G, Jensen GJ. 2011. Microtubules in bacteria: ancient tubulins build a five-protofilament homolog of the eukaryotic cytoskeleton. *PLoS Biol* 9:e1001213. <https://doi.org/10.1371/journal.pbio.1001213>.
- Swulius MT, Jensen GJ. 2012. The helical MreB cytoskeleton in *Escherichia coli* MC1000/pLE7 is an artifact of the N-Terminal yellow fluorescent protein tag. *J Bacteriol* 194:6382–6386. <https://doi.org/10.1128/JB.00505-12>.
- Gan L, Chen S, Jensen GJ. 2008. Molecular organization of Gram-negative peptidoglycan. *Proc Natl Acad Sci U S A* 105:18953–18957. <https://doi.org/10.1073/pnas.0808035105>.
- Beeby M, Gumbart JC, Roux B, Jensen GJ. 2013. Architecture and assembly of the Gram-positive cell wall. *Mol Microbiol* 88:664–672. <https://doi.org/10.1111/mmi.12203>.
- Ebersbach G, Briegel A, Jensen GJ, Jacobs-Wagner C. 2008. A self-associating protein critical for chromosome attachment, division, and polar organization in *Caulobacter*. *Cell* 134:956–968. <https://doi.org/10.1016/j.cell.2008.07.016>.
- Iancu CV, Ding HJ, Morris DM, Dias DP, Gonzales AD, Martino A, Jensen GJ. 2007. The structure of isolated *Synechococcus* strain WH8102 carboxysomes as revealed by electron cryotomography. *J Mol Biol* 372:764–773. <https://doi.org/10.1016/j.jmb.2007.06.059>.

12. Murphy GE, Leadbetter JR, Jensen GJ. 2006. In situ structure of the complete *Treponema primitia* flagellar motor. *Nature* 442:1062–1064. <https://doi.org/10.1038/nature05015>.
13. Chen S, Beeby M, Murphy GE, Leadbetter JR, Hendrixson DR, Briegel A, Li Z, Shi J, Tocheva EI, Muller A, Dobro MJ, Jensen GJ. 2011. Structural diversity of bacterial flagellar motors. *EMBO J* 30:2972–2981. <https://doi.org/10.1038/emboj.2011.186>.
14. Abrusci P, Vergara-Irigaray M, Johnson S, Beeby MD, Hendrixson DR, Roversi P, Friede ME, Deane JE, Jensen GJ, Tang CM, Lea SM. 2013. Architecture of the major component of the type III secretion system export apparatus. *Nat Struct Mol Biol* 20:99–104.
15. Chang YW, Rettberg LA, Treuner-Lange A, Iwasa J, Sogaard-Andersen L, Jensen GJ. 2016. Architecture of the type IVa pilus machine. *Science* 351:aad2001. <https://doi.org/10.1126/science.aad2001>.
16. Briegel A, Li X, Bilwes AM, Hughes KT, Jensen GJ, Crane BR. 2012. Bacterial chemoreceptor arrays are hexagonally packed trimers of receptor dimers networked by rings of kinase and coupling proteins. *Proc Natl Acad Sci U S A* 109:3766–3771. <https://doi.org/10.1073/pnas.1115719109>.
17. Tocheva EI, Matson EG, Morris DM, Moussavi F, Leadbetter JR, Jensen GJ. 2011. Peptidoglycan remodeling and conversion of an inner membrane into an outer membrane during sporulation. *Cell* 146:799–812. <https://doi.org/10.1016/j.cell.2011.07.029>.
18. Basler M, Pilhofer M, Henderson GP, Jensen GJ, Mekalanos JJ. 2012. Type VI secretion requires a dynamic contractile phage tail-like structure. *Nature* 483:182–186. <https://doi.org/10.1038/nature10846>.
19. Guerrero-Ferreira RC, Viollier PH, Ely B, Poindexter JS, Georgieva M, Jensen GJ, Wright ER. 2011. Alternative mechanism for bacteriophage adsorption to the motile bacterium *Caulobacter crescentus*. *Proc Natl Acad Sci U S A* 108:9963–9968. <https://doi.org/10.1073/pnas.1012388108>.
20. Oikonomou CM, Jensen GJ. 2016. A new view into prokaryotic cell biology from electron cryotomography. *Nat Rev Microbiol* 14:205–220. <https://doi.org/10.1038/nrmicro.2016.7>.
21. Ingerson-Mahar M, Briegel A, Werner JN, Jensen GJ, Gitai Z. 2010. The metabolic enzyme CTP synthase forms cytoskeletal filaments. *Nat cell biol* 12:739–746. <https://doi.org/10.1038/ncb2087>.
22. Briegel A, Ding HJ, Li Z, Werner J, Gitai Z, Dias DP, Jensen RB, Jensen GJ. 2008. Location and architecture of the *Caulobacter crescentus* chemoreceptor array. *Mol Microbiol* 69:30–41. <https://doi.org/10.1111/j.1365-2958.2008.06219.x>.
23. Chang YW, Chen S, Tocheva EI, Treuner-Lange A, Lobach S, Sogaard-Andersen L, Jensen GJ. 2014. Correlated cryogenic photoactivated localization microscopy and cryo-electron tomography. *Nat Methods* 11:737–739. <https://doi.org/10.1038/nmeth.2961>.
24. Murphy GE, Matson EG, Leadbetter JR, Berg HC, Jensen GJ. 2008. Novel ultrastructures of *Treponema primitia* and their implications for motility. *Mol Microbiol* 67:1184–1195. <https://doi.org/10.1111/j.1365-2958.2008.06120.x>.
25. Muller A, Beeby M, McDowall AW, Chow J, Jensen GJ, Clemons WM Jr. 2014. Ultrastructure and complex polar architecture of the human pathogen *Campylobacter jejuni*. *Microbiologyopen* 3:702–710.
26. Ding HJ, Oikonomou CM, Jensen GJ. 2015. The caltech tomography database and automatic processing pipeline. *J Struct Biol* 192:279–286. <https://doi.org/10.1016/j.jsb.2015.06.016>.
27. Dobro MJ, Piper A. 2017. Uncharacterized bacterial structures revealed by electron cryotomography. [figshare https://figshare.com/s/782461843c3150d27cfa](https://figshare.com/s/782461843c3150d27cfa). Retrieved 23 June 2017.
28. Staley JT, Bont JA, Jonge K. 1976. Prosthecobacter fusiformis nov. gen. et sp., the fusiform caulobacter. *Antonie Van Leeuwenhoek* 42:333–342. <https://doi.org/10.1007/BF00394132>.
29. Gonin M, Quardokus EM, O'Donnol D, Maddock J, Brun YV. 2000. Regulation of stalk elongation by phosphate in *Caulobacter crescentus*. *J Bacteriol* 182:337–347.
30. Wagner JK, Setayeshgar S, Sharon LA, Reilly JP, Brun YV. 2006. A nutrient uptake role for bacterial cell envelope extensions. *Proc Natl Acad Sci U S A* 103:11772–11777. <https://doi.org/10.1073/pnas.0602047103>.
31. Schlimpert S, Klein EA, Briegel A, Hughes V, Kahnt J, Bolte K, Maier UG, Brun YV, Jensen GJ, Gitai Z, Thanbichler M. 2012. General protein diffusion barriers create compartments within bacterial cells. *Cell* 151:1270–1282. <https://doi.org/10.1016/j.cell.2012.10.046>.
32. De Troch P, Vanderleyden J. 1996. Surface Properties and motility of rhizobium and azospirillum in relation to plant root attachment. *Microb Ecol* 32:149–169. <https://doi.org/10.1007/BF00185885>.
33. Steenhoudt O, Vanderleyden J. 2000. Azospirillum, a free-living nitrogen-fixing bacterium closely associated with grasses: genetic, biochemical and ecological aspects. *FEMS Microbiol Rev* 24:487–506. <https://doi.org/10.1111/j.1574-6976.2000.tb00552.x>.
34. Mukherjee T, Kumar D, Burriss N, Xie Z, Alexandre G. 2016. Azospirillum brasilense chemotaxis depends on two signaling pathways regulating cell-to-cell clumping parameters. *J Bacteriol* 198:1764–1772. <https://doi.org/10.1128/JB.00020-16>.
35. Bible AN, Khalsa-Moyers GK, Mukherjee T, Green CS, Mishra P, Purcell A, Aksenova A, Hurst GB, Alexandre G. 2015. Metabolic adaptations of *Azospirillum brasilense* to oxygen stress by cell-to-cell clumping and flocculation. *Appl Environ Microbiol* 81:8346–8357. <https://doi.org/10.1128/AEM.02782-15>.
36. Bible A, Russell MH, Alexandre G. 2012. The *Azospirillum brasilense* Che1 chemotaxis pathway controls swimming velocity, which affects transient cell-to-cell clumping. *J Bacteriol* 194:3343–3355. <https://doi.org/10.1128/JB.00310-12>.
37. Moissl C, Rachel R, Briegel A, Engelhardt H, Huber R. 2005. The unique structure of archaeal ‘hami’, highly complex cell appendages with nanograppling hooks. *Mol Microbiol* 56:361–370. <https://doi.org/10.1111/j.1365-2958.2005.04294.x>.
38. Epstein EA, Reizian MA, Chapman MR. 2009. Spatial clustering of the curlin secretion lipoprotein requires curli fiber assembly. *J Bacteriol* 191:608–615. <https://doi.org/10.1128/JB.01244-08>.
39. Van Gerven N, Klein RD, Hultgren SJ, Remaut H. 2015. Bacterial amyloid formation: Structural insights into curli biogenesis. *Trends Microbiol* 23:693–706. <https://doi.org/10.1016/j.tim.2015.07.010>.
40. Dueholm MS, Albertsen M, Otzen D, Nielsen PH. 2012. Curli functional amyloid systems are phylogenetically widespread and display large diversity in operon and protein structure. *PLoS One* 7:e51274. <https://doi.org/10.1371/journal.pone.0051274>.
41. Cameron DE, Urbach JM, Mekalanos JJ. 2008. A defined transposon mutant library and its use in identifying motility genes in *Vibrio cholerae*. *Proc Natl Acad Sci U S A* 105:8736–8741. <https://doi.org/10.1073/pnas.0803281105>.
42. Weiner RM, Melick M, O'Neill K, Quintero E. 2000. *Hyphomonas adhaerens* sp. nov., *Hyphomonas johnsonii* sp. nov. and *Hyphomonas rosenbergii* sp. nov., marine budding and prosthecate bacteria. *Int J Syst Evol Microbiol* 50 Part 2:459–469.
43. Zervas PM, Kessel M, Quintero EJ, Weiner RM. 1997. Fine-structure evidence for cell membrane partitioning of the nucleoid and cytoplasm during bud formation in *Hyphomonas* species. *J Bacteriol* 179:148–156. <https://doi.org/10.1128/jb.179.1.148-156.1997>.
44. Pommier Y, Covey JM, Kerrigan D, Markovits J, Pham R. 1987. DNA unwinding and inhibition of mouse leukemia L1210 DNA topoisomerase I by intercalators. *Nucleic Acids Res* 15:6713–6731. <https://doi.org/10.1093/nar/15.16.6713>.
45. Wolf SG, Frenkiel D, Arad T, Finkel SE, Kolter R, Minsky A. 1999. DNA protection by stress-induced biocrystallization. *Nature* 400:83–85. <https://doi.org/10.1038/21918>.
46. Teramoto J, Yoshimura SH, Takeyasu K, Ishihama A. 2010. A novel nucleoid protein of *Escherichia coli* induced under anaerobic growth conditions. *Nucleic Acids Res* 38:3605–3618. <https://doi.org/10.1093/nar/gkq077>.
47. Lim CJ, Lee SY, Teramoto J, Ishihama A, Yan J. 2013. The nucleoid-associated protein Dan organizes chromosomal DNA through rigid nucleoprotein filament formation in *E. coli* during anoxia. *Nucleic Acids Res* 41:746–753. <https://doi.org/10.1093/nar/gks1126>.
48. Egelman EH, Stasiak A. 1986. Structure of helical RecA-DNA complexes. Complexes formed in the presence of ATP-gamma-S or ATP. *J Mol Biol* 191:677–697.
49. Mizuno N, Dramicanin M, Mizuuchi M, Adam J, Wang Y, Han YW, Yang W, Steven AC, Mizuuchi K, Ramon-Maiques S. 2013. MuB is an AAA+ ATPase that forms helical filaments to control target selection for DNA transposition. *Proc Natl Acad Sci U S A* 110:E2441–E2450. <https://doi.org/10.1073/pnas.1309499110>.
50. Barry RM, Gitai Z. 2011. Self-assembling enzymes and the origins of the cytoskeleton. *Curr Opin Microbiol* 14:704–711. <https://doi.org/10.1016/j.mib.2011.09.015>.
51. Matayoshi S, Oda H, Sarwar G. 1989. Relationship between the production of spirosomes and anaerobic glycolysis activity in *Escherichia coli* B. *J Gen Microbiol* 135:525–529.
52. Laurenceau R, Krasteva PV, Diallo A, Ouarti S, Duchateau M, Malosse C, Chamot-Rooke J, Fronzes R. 2015. Conserved *Streptococcus pneumoniae*

- moniae* spiroosomes suggest a single type of transformation pilus in competence. PLoS Pathog 11:e1004835. <https://doi.org/10.1371/journal.ppat.1004835>.
53. Swulius MT, Chen S, Jane Ding H, Li Z, Briegel A, Pilhofer M, Tocheva EI, Lybarger SR, Johnson TL, Sandkvist M, Jensen GJ. 2011. Long helical filaments are not seen encircling cells in electron cryotomograms of rod-shaped bacteria. Biochem Biophys Res Commun 407:650–655. <https://doi.org/10.1016/j.bbrc.2011.03.062>.
 54. Jones LJ, Carballido-Lopez R, Errington J. 2001. Control of cell shape in bacteria: helical, actin-like filaments in *Bacillus subtilis*. Cell 104:913–922. [https://doi.org/10.1016/S0092-8674\(01\)00287-2](https://doi.org/10.1016/S0092-8674(01)00287-2).
 55. Shih YL, Le T, Rothfield L. 2003. Division site selection in *Escherichia coli* involves dynamic redistribution of Min proteins within coiled structures that extend between the two cell poles. Proc Natl Acad Sci U S A 100:7865–7870. <https://doi.org/10.1073/pnas.1232225100>.
 56. Scheffel A, Gruska M, Faivre D, Linaroudis A, Plietzko JM, Schuler D. 2006. An acidic protein aligns magnetosomes along a filamentous structure in magnetotactic bacteria. Nature 440:110–114. <https://doi.org/10.1038/nature04382>.
 57. Szwedziak P, Wang Q, Bharat TA, Tsim M, Lowe J. 2014. Architecture of the ring formed by the tubulin homologue FtsZ in bacterial cell division. eLife 9:e04601. doi:<https://doi.org/10.7554/elife.04601>.
 58. Kuhn J, Briegel A, Morschel E, Kahnt J, Leser K, Wick S, Jensen GJ, Thanbichler M. 2010. Bactofilins, a ubiquitous class of cytoskeletal proteins mediating polar localization of a cell wall synthase in *Caulobacter crescentus*. EMBO J 29:327–339. <https://doi.org/10.1038/emboj.2009.358>.
 59. Aylett CH, Wang Q, Michie KA, Amos LA, Lowe J. 2010. Filament structure of bacterial tubulin homologue TubZ. Proc Natl Acad Sci U S A 107:19766–19771. <https://doi.org/10.1073/pnas.1010176107>.
 60. Bharat TA, Murshudov GN, Sachse C, Lowe J. 2015. Structures of actin-like ParM filaments show architecture of plasmid-segregating spindles. Nature 523:106–110. <https://doi.org/10.1038/nature14356>.
 61. Santarella-Mellwig R, Franke J, Jaedicke A, Gorjanacz M, Bauer U, Budd A, Mattaj JW, Devos DP. 2010. The compartmentalized bacteria of the Planctomycetes-Verrucomicrobia-Chlamydiae superphylum have membrane coat-like proteins. PLoS biology 8:e1000281. <https://doi.org/10.1371/journal.pbio.1000281>.
 62. Lonhienne TG, Sagulenko E, Webb RI, Lee KC, Franke J, Devos DP, Nouwens A, Carroll BJ, Fuerst JA. 2010. Endocytosis-like protein uptake in the bacterium *Gemmata obscuriglobus*. Proc Natl Acad Sci U S A 107:12883–12888. <https://doi.org/10.1073/pnas.1001085107>.
 63. Makarova KS, Koonin EV. 2010. Two new families of the FtsZ-tubulin protein superfamily implicated in membrane remodeling in diverse bacteria and archaea. Biol Direct 5:33. <https://doi.org/10.1186/1745-6150-5-33>.
 64. Briegel A, Ortega DR, Tocheva EI, Wuichet K, Li Z, Chen S, Müller A, Iancu CV, Murphy GE, Dobro MJ, Zhulin IB, Jensen GJ. 2009. Universal architecture of bacterial chemoreceptor arrays. Proc Natl Acad Sci U S A 106:17181–17186. <https://doi.org/10.1073/pnas.0905181106>.
 65. Briegel A, Ortega DR, Mann P, Kjær A, Ringgaard S, Jensen GJ. 2016. Chemotaxis cluster 1 proteins form cytoplasmic arrays in *Vibrio cholerae* and are stabilized by a double signaling domain receptor DosM. Proc Natl Acad Sci U S A 113:10412–10417. <https://doi.org/10.1073/pnas.1604693113>.
 66. Briegel A, Ames P, Gumbart JC, Oikonomou CM, Parkinson JS, Jensen GJ. 2013. The mobility of two kinase domains in the *Escherichia coli* chemoreceptor array varies with signalling state. Mol Microbiol 89:831–841. <https://doi.org/10.1111/mmi.12309>.
 67. Briegel A, Beeby M, Thanbichler M, Jensen GJ. 2011. Activated chemoreceptor arrays remain intact and hexagonally packed. Mol Microbiol 82:748–757. <https://doi.org/10.1111/j.1365-2958.2011.07854.x>.
 68. Cserti E, Roskopf S, Chang YW, Eisheuer S, Selter L, Shi J, Regh C, Koert U, Jensen GJ, Thanbichler M. 2017. Dynamics of the peptidoglycan biosynthetic machinery in the stalked budding bacterium *Hyphomonas neptunium*. Mol Microbiol 103:875–895. <https://doi.org/10.1111/mmi.13593>.
 69. Tivol WF, Briegel A, Jensen GJ. 2008. An improved cryogen for plunge freezing. Microsc Microanal 14:375–379. <https://doi.org/10.1017/S1431927608080781>.
 70. Suloway C, Shi J, Cheng A, Pulokas J, Carragher B, Potter CS, Zheng SQ, Agard DA, Jensen GJ. 2009. Fully automated, sequential tilt-series acquisition with Legion. J Struct Biol 167:11–18. <https://doi.org/10.1016/j.jsb.2009.03.019>.
 71. Zheng SQ, Keszthelyi B, Branlund E, Lyle JM, Braunfeld MB, Sedat JW, Agard DA. 2007. UCSF tomography: an integrated software suite for real-time electron microscopic tomographic data collection, alignment, and reconstruction. J Struct Biol 157:138–147. <https://doi.org/10.1016/j.jsb.2006.06.005>.
 72. Kremer JR, Mastrorade DN, McIntosh JR. 1996. Computer visualization of three-dimensional image data using IMOD. J Struct Biol 116:71–76. <https://doi.org/10.1006/jsbi.1996.0013>.
 73. Amat F, Moussavi F, Comolli LR, Elidan G, Downing KH, Horowitz M. 2008. Markov random field based automatic image alignment for electron tomography. J Struct Biol 161:260–275. <https://doi.org/10.1016/j.jsb.2007.07.007>.
 74. Nicastro D, Schwartz C, Pierson J, Gaudette R, Porter ME, McIntosh JR. 2006. The molecular architecture of axonemes revealed by cryoelectron tomography. Science 313:944–948. <https://doi.org/10.1126/science.1128618>.
 75. Piper AT. 2017. Cell visualization VR. <https://play.google.com/store/apps/details?id=com.BishopVisual.Mk2&rdid=com.BishopVisual.Mk2>. Retrieved 23 June 2017.